SCIENCE CHINA
Information Sciences

• RESEARCH PAPER •

February 2026, Vol. 69, Iss. 2, 122402:1–122402:7
https://doi.org/10.1007/s11432-025-4527-1

High linearity and high-power of composite component graded-AlGaN/graded-InGaN/ GaN HEMTs

Qian YU[1], Ling YANG[1*], Long ZHANG[1], Chunzhou SHI[2], Bin HOU[1*], Mei WU[1], Meng ZHANG[1], Hao LU[1], Xu ZOU[1], Wenze GAO[1], Xiaohua MA[1] & Yue HAO[1]

[1]*State Key Discipline Laboratory of Wide Band-gap Semiconductor Technology, School of Microelectronics, Xidian University, Xi'an 710071, China*
[2]*School of Advanced Materials and Nanotechnology, Xidian University, Xi'an 710071, China*

Received 8 April 2025/Revised 19 June 2025/Accepted 23 July 2025/Published online 4 January 2026

Abstract In this paper, the composite graded-AlGaN/graded-InGaN high electron mobility transistors (CG-HEMTs) are reported with high linearity and high power. In order to broaden the electron distribution, the graded-AlGaN barrier and graded-InGaN channel layer are combined. Thus, the wider gate voltage swing (GVS) is realized. At the same time, due to the two graded layers, the centroid of 3DEG in CG-HEMTs is located in the middle of the two graded layers. Thus, the centroid of 3DEG of the CG-HEMTs is kept away from both the high Al component and the high In component. The random alloy scattering of charge carriers is reduced. This is why the mobility of the CG-HEMTs is higher. While the transconductance ($g_{\rm m}$) of CG-HEMTs is broadened, the peak $g_{\rm m}$ of the CG-HEMTs is higher because of the high mobility. In order to achieve high power, the high Al component graded-AlGaN (40%–0%) is grown to enhance polarization. Ultimately, the 4 V of GVS, 260 mS/mm, and 1370 mA/mm are achieved by the CG-HEMTs. At 3.6 GHz, the 6.2 W/mm of output power density ($P_{\rm out}$) and 55% of power-added efficiency (PAE) are realized. The output third-order intercept point (OIP3) of the CG-HEMTs is 40.9 dBm, which is the highest OIP3 ever reported.

Keywords GaN, AlGaN/GaN HEMTs, graded-AlGaN, graded-InGaN, high linearity

Citation Yu Q, Yang L, Zhang L, et al. High linearity and high-power of composite component graded-AlGaN/graded-InGaN/GaN HEMTs. Sci China Inf Sci, 2026, 69(2): 122402, https://doi.org/10.1007/s11432-025-4527-1

1 Introduction

Gallium nitride (GaN) high electron mobility transistors (HEMTs) have characteristics that display a wide bandgap, high critical breakdown electric field, and high electron saturation speed, and have been developed in the past decades [1–4]. The GaN HEMTs are not only successfully applied to 5G communication base stations but also can be applied to mobile terminals [5]. However, linearity has always been a key issue restricting the development and application of GaN HEMTs. The reasons for the low linearity of the GaN HEMTs are the non-linear source access resistance ($r_{\rm s}$) [6] and the lower saturation velocity ($v_{\rm sat}$) at high drain current ($I_{\rm d}$) density [7,8].

After previous studies, the linearity could be improved by polarization-graded HEMTs (Pol-HEMTs) [9,10]. The $r_{\rm s}$-$I_{\rm d}$ relationship can be modulated by the Pol-HEMTs. The decrease in $v_{\rm sat}$ is suppressed by the voltage increase because of the three-dimensional electronic gas (3DEG) in Pol-HEMTs [11]. It has been shown that both graded-AlGaN [12] and graded-InGaN [13] could increase the gate voltage swing (GVS) of the GaN HEMTs. However, on the one hand, the requirements for GaN HEMTs linearity are higher by the development of communication. On the other hand, the polarization of Pol-HEMTs is weak, resulting in lower output current ($I_{\rm d}$) and output power density ($P_{\rm out}$).

To further improve the linearity of the GaN HEMTs, the graded-AlGaN barrier layer and graded-InGaN graded channel layer are combined in this article. The carrier distribution is further broadened. Thus, the wider GVS could be achieved. Further, the higher linearity could be realized by the composite graded-AlGaN/graded-InGaN high electron mobility transistors (CG-HEMTs). In [14], the Si-doped graded-AlGaN barrier layer was used to improve the carrier density. However, the Si-doped barrier layer results in a serious leakage current. Thus, the Si-doped barrier layer could only be used for low voltage applications. In order to improve $P_{\rm out}$ of the graded barrier layer, the Al component of the graded barrier layer is defined as 40%–0% (from top to bottom). The strong polarization

* Corresponding author (email: yangling@xidian.edu.cn, houbinme@163.com)

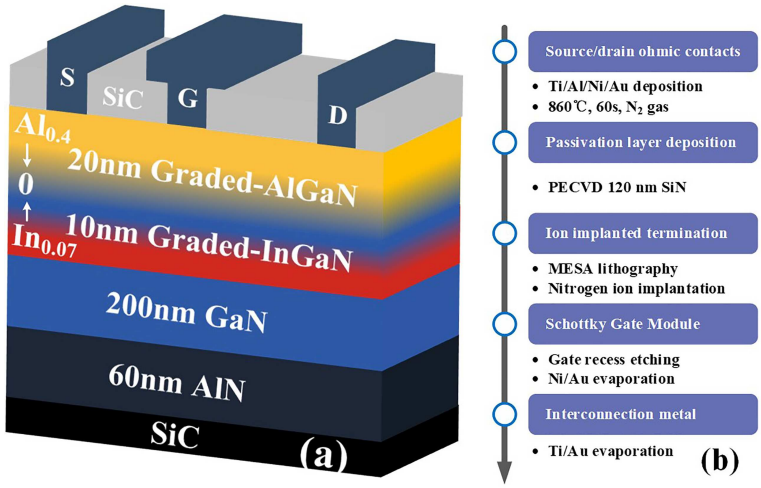

Figure 1 (Color online) (a) Schematic cross section of the CG-HEMTs; (b) process flow for the fabricated CG-HEMTs.

can be achieved by a higher Al component [15,16]. Meanwhile, the graded-AlGaN causes the centroid of 3DEG to shift upward [14], and the graded-InGaN leads the centroid of 3DEG to shift downward [17]. Thus, the centroid of 3DEG of the CG-HEMTs is located in the middle of the two graded layers. The center of 3DEG is far away from the high Al component and the high In component. Thus, the random alloy scattering is reduced. Therefore, the mobility of the CG-HEMTs is improved. Further, the higher $I_{\rm d}$ and peak $g_{\rm m}$ are realized. Due to the higher $I_{\rm d}$ and wider GVS, the high linearity and $P_{\rm out}$ could be achieved by the CG-HEMTs at the same time. In conclusion, the carrier distribution is broadened by the CG-HEMTs to improve the linearity. The high Al component of the graded barrier layer is defined to improve $I_{\rm d}$. The centroid of 3DEG of the CG-HEMTs is located in the middle of the two graded layers to improve the mobility.

In this paper, the graded-AlGaN/graded-InGaN/GaN/AlN HEMTs are designed and fabricated for high linearity and high power application. The 4 V of GVS is realized. The saturation current ($I_{\rm d,max}$) and peak $g_{\rm m}$ are 1370 mA/mm and 260 mS/mm, respectively. Meanwhile, the current gain cutoff frequency ($f_{\rm T}$) and the maximum oscillation frequency ($f_{\rm max}$) are 26.3 and 51.5 GHz at a drain voltage ($V_{\rm d}$) of 10 V, respectively. The 6.2 W/mm of output power density ($P_{\rm out}$) and 55% of power-added efficiency (PAE) are achieved at 3.6 GHz and $V_{\rm D}$ = 28 V. And, the state-of-the-art 40.9 dBm of OIP3 is achieved.

2 Growth epitaxy and device fabrication

The 3-inch semi-insulating 4H-SiC was used as substrates. And the epitaxial layers of the CG-HEMTs were grown by metal organic chemical vapor deposition (MOCVD), including a 60 nm high-quality AlN buffer layer, a 200 nm GaN channel layer and a 10 nm graded InGaN (0%–7%, from top to bottom) channel layer and a 20 nm graded-AlGaN (40%–0%, from top to bottom) barrier layer from down to top. By the Hall measurements, the electron density of the CG-HEMTs is 1.35×10^{13} cm^{-2}. The schematic cross section of the CG-HEMTs is shown in Figure 1(a).

The CG-HEMTs fabrication process started with depositing a metal stack including Ti/Al/Ni/Au. To form the ohmic contact, the CG-HEMTs are annealed at 860°C for 60 s in the N_2 ambiance. Then, the nitrogen ion implantation was used to form the CG-HEMTs electrical isolation. The CG-HEMTs are deposited SiN passivation by plasma-enhanced chemical vapor deposition (PECVD). Next, the lithography and CF4-based plasma etching are used to define the 0.5 μm gate window and the 1.3 μm gate cap, to achieve a T-shaped gate. The Schottky contact is achieved by Ni/Au metal stack. Finally, the interconnection of the CG-HEMTs is achieved by Ti/Au metal stack. The source-drain spacing ($L_{\rm sd}$) of the CG-HEMTs is 4 μm. The gate width is 2×50 μm. The process flow is shown in Figure 1(b).

3 Results and discussion

The capacitance vs. voltage (CV) characteristics and electron distribution profile of the CG-HEMTs are shown in Figure 2(a). The CV curve first shows a plateau, and then the capacitance increases linearly as the voltage increases.

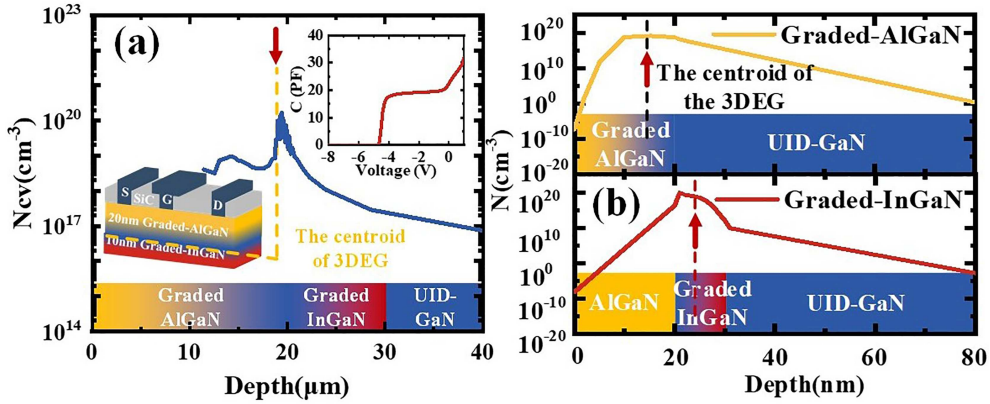

Figure 2 (Color online) (a) Capacitance-voltage and electron distribution profile of the CG epilayer; (b) schematic of the position of the three-dimensional electron gas centroid of the graded-AlGaN/graded-InGaN HEMTs.

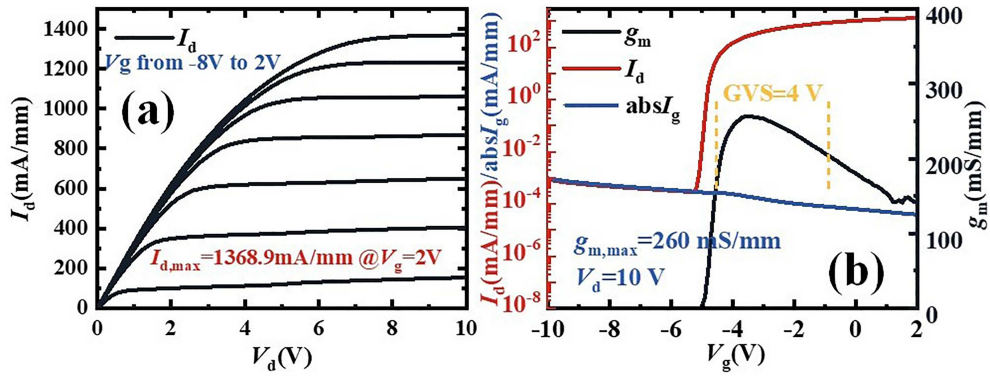

Figure 3 (Color online) (a) Output characteristics and (b) transfer curves of the CG-HEMTs.

Due to the two graded layers, the electron distribution exhibits two flat peaks. Due to the high Al component, the high carrier density is achieved. The schematic of the 3DEG centroid of the CG-HEMTs is shown in Figure 2(a). The electron concentration distributions and the centroid of the 3DEG of the graded-AlGaN/InGaN HEMTs are shown in Figure 2(b). It can be seen that the 3DEG centroid of the graded-AlGaN HEMTs is upper, that of the graded-InGaN HEMTs is lower, and that of the CG-HEMTs is middle. Thus, the random alloy scattering of the CG-HEMTs is reduced.

The output characteristics of the CG-HEMTs are shown in Figure 3(a). The $I_{d,max}$ of the CG-HEMTs is 1368.9 mA/mm, because of the high carrier density. The high P_{out} could be achieved by the high $I_{d,max}$. The transfer curve of the CG-HEMTs is shown in Figure 3(b). The threshold voltage (V_{TH}) of the CG-HEMTs is −4.8 V. Due to the 3DEG, the v_{sat} could stay constant by the voltage increased [10]. Thus, the g_m drop slows down by the gate voltage (V_g) increases, and the flatter g_m curve could be achieved. The 4 V of GVS could be realized by the CG-HEMTs. Thus, the high OIP3 could be achieved by the CG-HEMTs.

The contact resistance (R_c) and sheet resistance (R_{sheet}) of the CG-HEMTs are measured by the transmission line method (TLM). As shown in Figure 4(a), the 0.4 Ω·mm of average R_c and 294.7 Ω/sq of the average R_{sheet} are achieved by the annealing process. For the surface with high Al components, the R_c and R_{sheet} are low enough to achieve high P_{out}. To measure the current collapse (CC) of the CG-HEMTs, the pulse tests of different quiescent bias voltages are tested in Figure 4(b). The pulse width and period of the CG-HEMTs are 500 ns and 1 ms, respectively. As the drain quiescent bias voltage is 20 V, the CC of the CG-HEMTs is 3.82%. This is due to the high quality of the AlN buffer and passivation SiN layer [18]. Due to the low CC, the high PAE and P_{out} could be achieved by the CG-HEMTs.

As shown in Figure 5(a), the mobility of the CG-HEMTs is measured by the transfer curve at V_d = 0.1 V. The 1510 cm^2/(V·s) of mobility is realized by the CG-HEMTs, which benefits from the low random alloy scattering. Thus, the mobility of the CG-HEMTs is higher than that of the graded-AlGaN/InGaN HEMTs. In order to demonstrate the superiority of CG-HEMTs, the g_m of the CG-HEMTs and graded-AlGaN/InGaN is shown in Figure 5(b). The first derivative (g'_m) and second derivative (g''_m) of g_m of the CG-HEMTs and graded-AlGaN/InGaN are shown in Figures 5(c) and (d), respectively. The widest g_m curve could be achieved by the

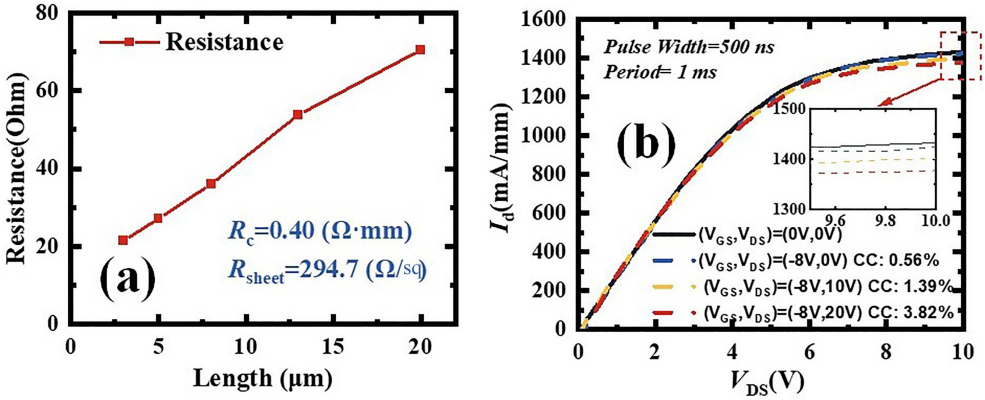

Figure 4 (Color online) (a) Transmission line method characteristics of the CG-HEMTs; (b) pulse characteristic curves of the CG-GaN HEMTs under (0, 0), (−8, 0), (−8, 10), and (−8, 20).

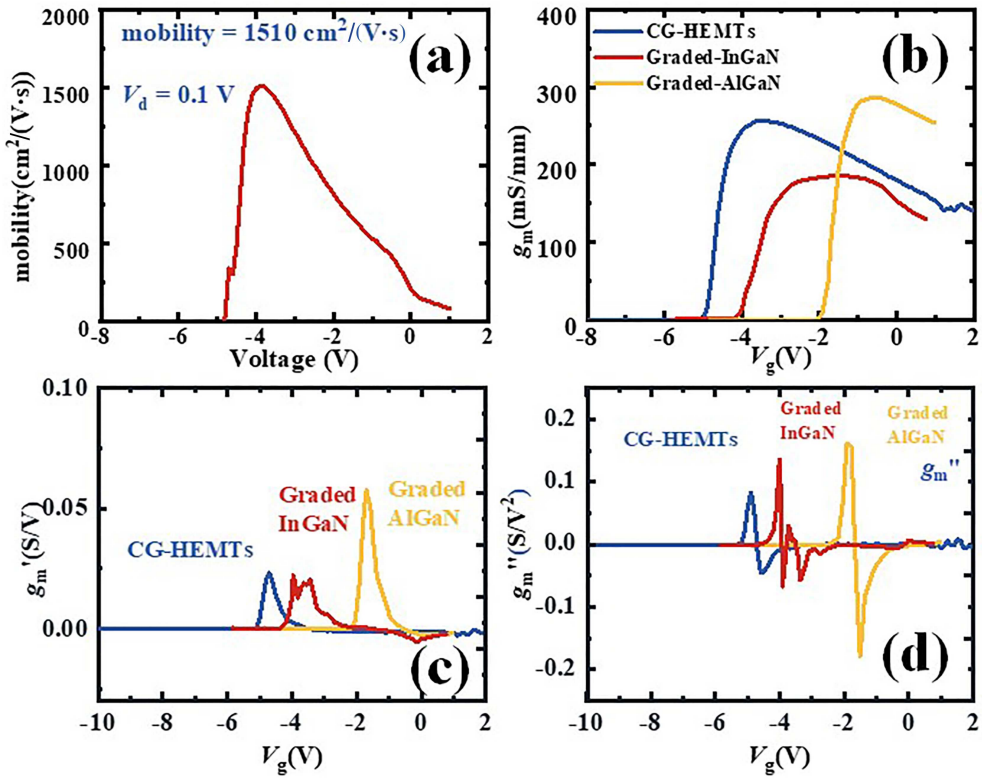

Figure 5 (Color online) (a) Mobility of the CG-HEMTs; (b) transconductance curves of the CG-GaN HEMTs and graded-InGaN/AlGaN HEMTs; (c) the first derivative of the transconductance curve of the CG-GaN HEMTs and graded-InGaN/AlGaN HEMTs; (d) the second derivative of the transconductance curve of the CG-GaN HEMTs and graded-InGaN/AlGaN HEMTs.

CG-HEMTs. It can be seen that the lowest $g'_{\rm m}$ and $g''_{\rm m}$ are achieved by the CG-HEMTs. According to Eq. (1) [19], we have the following.

To demonstrate that CG-HEMTs have smaller random alloy scattering, the intrinsic $g_{\rm m}$ of the GaN HEMTs is measured. The scattering parameters (S-parameters) were measured by the N5247B PNA-X network analyzer with IC characterization and analysis program (IC-CAP) [11, 20, 21]. As shown in Figure 6, the peak intrinsic $g_{\rm m}$ of the CG-HEMTs is 361 mS/mm. The peak intrinsic $g_{\rm m}$s of the graded-AlGaN/InGaN GaN HEMTs are 353 and 278 mS/mm, respectively. The threshold voltage ($V_{\rm th}$) corresponding to the intrinsic $g_{\rm m}$s curve is the same as the tested $g_{\rm m}$ curve in Figure 5(b). Compared with the graded-InGaN and graded-AlGaN GaN HEMTs, the CG-HEMTs have a higher intrinsic $g_{\rm m}$. This benefits from reduced random alloy scattering. The intrinsic $g_{\rm m}$ curve of the CG-HEMTs is wider than that of the graded-InGaN and graded-AlGaN HEMTs. This proves that the high linearity could be achieved by the CG-HEMTs.

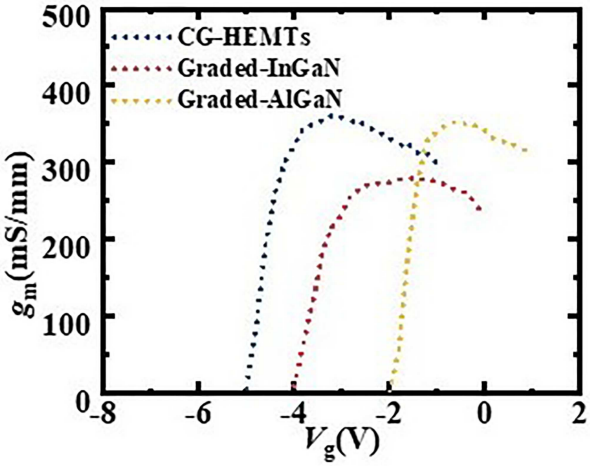

Figure 6 (Color online) Intrinsic g_ms of CG-HEMTs and graded-AlGaN/InGaN GaN HEMTs.

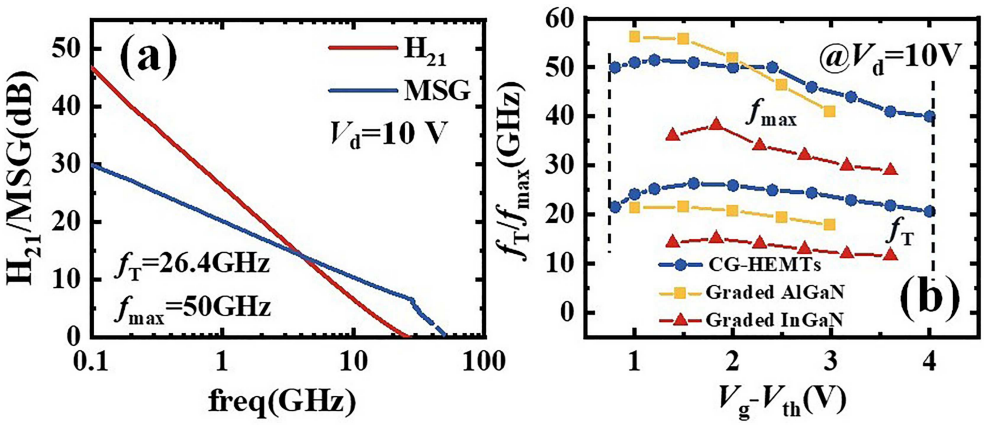

Figure 7 (Color online) (a) Small signal characteristics of the CG-HEMTs at V_d = 10 V; (b) V_g-V_{th} dependence of f_T and f_{max} measured at V_d = 10 V of the CG-HEMTs and graded-AlGaN/InGaN.

The current gain (H_{21}) and maximum stable gain (MSG) of the CG-HEMTs are shown in Figure 7(a). The small signal characteristics of the CG-HEMTs are tested at V_d = 10 V. The f_T and f_{max} are 26.4 and 50.0 GHz, respectively. The f_T is higher than the other GaN HEMTs for the L_g of 0.5 μm. Because of the high g_m, the high f_T could be achieved by the CG-HEMTs. The f_T and f_{max} at V_d of 10 V vs. V_g-V_{th} are shown in Figure 7(b). It can be seen that the curves of the f_T and f_{max} remain flat in the V_g-V_{th} range of 1–4 V. Meanwhile, the f_T/f_{max} curve of the CG-HEMTs is flatter and higher than that of the graded-AlGaN/InGaN. It benefits from the flatter g_m curve. Thus, this also demonstrates the potential of CG-HEMTs for high linearity [5].

As shown in Figure 8(a), the load-pull measurement for the CG-HEMTs is tested at 3.6 GHz and V_d = 28 V. Due to the high $I_{d,max}$, the 5.5 W/mm of P_{out} could be achieved. The PAE of the CG-HEMTs is 53%. The flat gain curve benefits from the wider GVS. The 1 dB compression point (P1dB) of the CG-HEMTs is 25 dBm. This shows the high linearity for the CG-HEMTs [22]. The I_{out} of the CG-HEMTs is shown. In Figure 8(b), the two-tone linearity of the CG-HEMTs is tested at 3.6 GHz fundamental frequency and 3.61 GHz 2nd tone frequency. The OIP3 and OIP3/P_{DC} of the CG-HEMTs are 40.9 dBm and 13 dB, respectively.

In Figure 9(a), the benchmarks of OIP3 versus $I_{d,max}$ for the CG-HEMTs against graded-AlGaN/graded-InGaN GaN HEMTs in other studies [9,11,13,14,23] are shown. It can be seen that the highest $I_{d,max}$ and OIP3 are achieved by the CG-HEMTs. Meanwhile, the benchmarks of OIP3 versus P_{out} are shown in Figure 9(b). Due to the high Al component improved the density of the carrier, the higher P_{out} could be achieved by the CG-HEMTs. This proves that the CG-HEMTs could meet the needs of both high linearity and high power applications. It provides a new idea for the design of the epitaxial layers of the GaN HEMTs in the future.

To demonstrate the advantages of this work, Table 1 is made to compare high-linearity GaN HEMTs in different studies [9,11,14,17,24–26]. It could be seen that the OIP3 and P_{out} of the CG-HEMTs are state-of-the-art work. This benefits from a widened carrier distribution, improved mobility, and saturation currents.

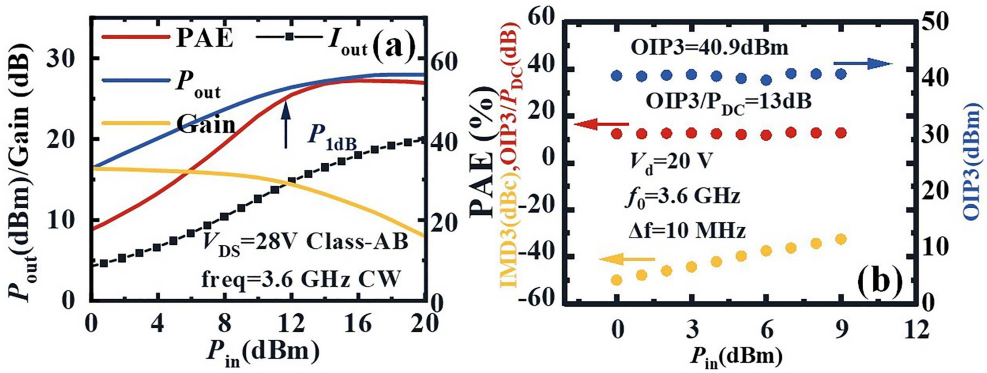

Figure 8 (Color online) (a) Load-pull measurement for the CG-HEMTs at 3.6 GHz and V_d = 65 V; (b) the benchmarks of two-tone linearity measurements with f_1 = 3.6 GHz and f_2 = 3.61 GHz biased near Class A.

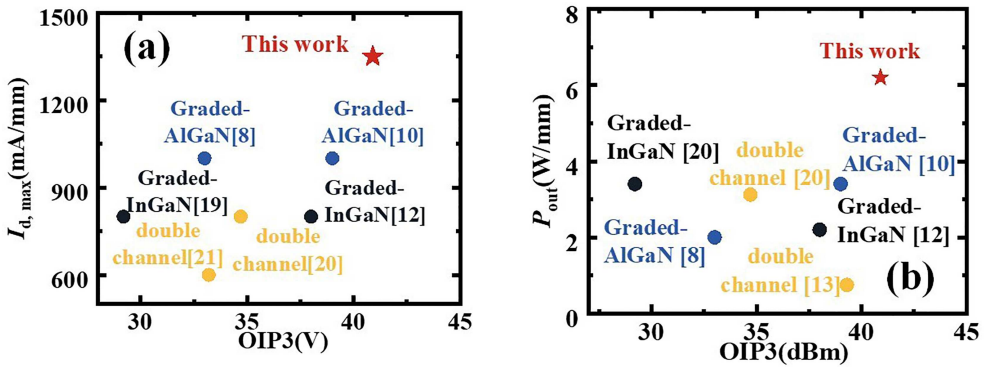

Figure 9 (Color online) (a) OIP3 versus $I_{d,max}$ and (b) OIP3 versus P_{out} for the CG-HEMTs against graded-AlGaN/graded-InGaN GaN HEMTs in other literature.

Table 1 Comparison of linearity characteristics of high linearity GaN HEMTs in different studies.

	$I_{d,max}$ (mA/mm)	GVS (V)	OIP3 (dBm)	OIP3/P_{DC} (dB)	P_{out} (W/mm)
This work	1370	4	40.9	13	6.4
HKUST [24]	900	5.5	33.2	–	3.38
Ohio [9]	720	2.5	33	12	2
Ohio [11]	1000	3	39	13.3	3.4
XD [14]	1900	6.5	39.3	10	0.75
XD [25]	970	3.5	36.4	12.9	–
UCSB [26]	1500	–	–	12	3
UCSB [17]	1550	2.5	32	15	–

4 Conclusion

In this paper, GaN HEMTs are reported with a high Al component graded-AlGaN barrier and a graded InGaN channel layer. The CG-HEMTs could meet the needs of high linearity and high power at the same time. The distribution of 3DEG is broadened by the two graded layers. Thus, the wider GVS is realized by the CG-HEMTs. The mobility of the CG-HEMTs is improved, because the centroid of 3DEG in CG-HEMTs is far away from the high Al component and the high In component. The random alloy scattering is reduced by the middle location of the centroid of 3DEG in CG-HEMTs. The high Al component strengthens polarization, which increases the carrier density. Thus, the higher P_{out} could be achieved by the CG-HEMTs. The state-of-the-art 40.9 dBm OIP3 is realized. This proves that the CG-HEMTs could meet the needs of high linearity and high power applications at the same time.

Acknowledgements This work was supported in part by National Natural Science Foundation of China (Grant Nos. 62090014, 62234009, 62188102, 62104179, 62104184, 62131014, 62104178), China National Postdoctoral Program for Innovative Talents (Grant No. BX20200262), and China Postdoctoral Science Foundation (Grant Nos. 2021M692499, 2022T150505).

References

1 Hao Y, Yang L, Ma X, et al. High-performance microwave gate-recessed AlGaN/AlN/GaN MOS-HEMT with 73% power-added efficiency. IEEE Electron Device Lett, 2011, 32: 626–628
2 Shi C Z, Yang L, Zhang M, et al. Improved RF power performance via electrostatic shielding effect using AlGaN/GaN/graded-AlGaN/GaN double-channel structure. Sci China Inf Sci, 2024, 67: 149401
3 Chang Q Y, Hou B, Yang L, et al. High-voltage quasi-vertical GaN-on-Si Schottky barrier diode with edge termination structure of optimized multi-level N ion implantation. Sci China Inf Sci, 2024, 67: 229402
4 Chen Y L, Zhu Q, Zhu J J, et al. Degradation induced by holes in Si_3N_4/AlGaN/GaN MIS HEMTs under off-state stress with UV light. Sci China Inf Sci, 2023, 66: 122401
5 Zheng Z, Song W, Lei J, et al. GaN HEMT with convergent channel for low intrinsic knee voltage. IEEE Electron Device Lett, 2020, 41: 1304–1307
6 Palacios T, Rajan S, Chakraborty A, et al. Influence of the dynamic access resistance in the g_m and f_T linearity of AlGaN/GaN HEMTs. IEEE Trans Electron Devices, 2005, 52: 2117–2123
7 Khurgin J B, Bajaj S, Rajan S. Amplified spontaneous emission of phonons as a likely mechanism for density-dependent velocity saturation in GaN transistors. Appl Phys Express, 2016, 9: 094101
8 Bajaj S, Yang Z, Akyol F, et al. Graded AlGaN channel transistors for improved current and power gain linearity. IEEE Trans Electron Devices, 2017, 64: 3114–3119
9 Sohel S H, Xie A, Beam E, et al. X-band power and linearity performance of compositionally graded AlGaN channel transistors. IEEE Electron Device Lett, 2018, 39: 1884–1887
10 Moon J S, Wong J, Grabar B, et al. 360 GHz f_{MAX} graded-channel AlGaN/GaN HEMTs for mmW low-noise applications. IEEE Electron Device Lett, 2020, 41: 1173–1176
11 Sohel S H, Rahman M W, Xie A, et al. Linearity improvement with AlGaN polarization- graded field effect transistors with low pressure chemical vapor deposition grown SiN_x passivation. IEEE Electron Device Lett, 2019, 41: 19–22
12 Ancona M G, Calame J P, Meyer D J, et al. Compositionally graded III-N HEMTs for improved linearity: a simulation study. IEEE Trans Electron Devices, 2019, 66: 2151–2157
13 Sohel S H, Xie A, Beam E, et al. Polarization engineering of AlGaN/GaN HEMT with graded InGaN sub-channel for high-linearity X-band applications. IEEE Electron Device Lett, 2019, 40: 522–525
14 Yu Q, Shi C, Yang L, et al. High current and linearity AlGaN/GaN/-graded-AlGaN:Si-doped/GaN heterostructure for low voltage power amplifier application. IEEE Electron Device Lett, 2023, 44: 582–585
15 Heikman S, Keller S, Wu Y, et al. Polarization effects in AlGaN/GaN and GaN/AlGaN/GaN heterostructures. J Appl Phys, 2003, 93: 10114–10118
16 Smorchkova I P, Elsass C R, Ibbetson J P, et al. Polarization-induced charge and electron mobility in AlGaN/GaN heterostructures grown by plasma-assisted molecular-beam epitaxy. J Appl Phys, 1999, 86: 4520–4526
17 Shrestha P, Guidry M, Romanczyk B, et al. High linearity and high gain performance of N-Polar GaN MIS-HEMT at 30 GHz. IEEE Electron Device Lett, 2020, 41: 681–684
18 Yang L, Jia F, Lu H, et al. Record power performance of 33.1 W/mm with 62.9% PAE at X-band and 14.4 W/mm at Ka-band from AlGaN/GaN/AlN:Fe heterostucture. In: Proceedings of 2023 International Electron Devices Meeting (IEDM), 2023. 1–4
19 Greenberg D R, Del Alamo J A. Nonlinear source and drain resistance in recessed-gate heterostructure field-effect transistors. IEEE Trans Electron Devices, 1996, 43: 1304–1306
20 Chen G, Kumar V, Schwindt R S, et al. A low gate bias model extraction technique for AlGaN/GaN HEMTs. IEEE Trans Microwave Theor Techn, 2006, 54: 2949–2953
21 Crupi G, Xiao D, Schreurs D M M P, et al. Accurate multibias equivalent-circuit extraction for GaN HEMTs. IEEE Trans Microwave Theor Techn, 2006, 54: 3616–3622
22 Lai R, Grundbacher R, Barsky M, et al. Extremely high P1dB MMIC amplifiers for Ka-band applications. In: Proceedings of Annual IEEE Symposium on Gallium Arsenide Integrated Circuit (GaAs IC), 2001. 115–117
23 Liu J, Zhou Y, Zhu J, et al. DC and RF characteristics of AlGaN/GaN/InGaN/GaN double-heterojunction HEMTs. IEEE Trans Electron Devices, 2006, 54: 2–10
24 Liu J, Zhou Y G, Chu R M, et al. Highly linear $Al_{0.3}Ga_{0.7}N$-$Al_{0.05}Ga_{0.95}N$-GaN composite-channel HEMTs. IEEE Electron Device Lett, 2005, 26: 145–147
25 Lu H, Deng L, Yang L, et al. High power linearity and low leakage current of AlN/GaN/InGaN coupling channel HEMTs with N_2O oxidation treatment. IEEE Electron Device Lett, 2024, 45: 960–963
26 Arias A, Rowell P, Bergman J, et al. High performance N-polar GaN HEMTs with OIP3/Pdc ∼12 dB at 10 GHz. In: Proceedings of 2017 IEEE Compound Semiconductor Integrated Circuit Symposium (CSICS), 2017. 1–3